THE EXPLOITATION OF X-RAY DIFFRACTION IN CHARACTERIZATION OF STRENGTH OF HOT-ROLLED AND COLD-DRAWN FERRITIC-PEARLITIC STEEL

D. Šimek[1], D. Rafaja[1], M. Motylenko[1], V. Klemm[1], C. Ullrich[1], A. Oswald[2], R. Schmidtchen[2] and G. Lehmann[2]

[1]Institute of Materials Science, TU Bergakademie Freiberg, D-09599 Freiberg, Germany
[2]Materials Forming Institute, TU Bergakademie Freiberg, D-09599 Freiberg, Germany
simek@fzu.cz

Keywords:
Ferritic-pearlitic steels, X-ray diffraction, ultimate tensile strength, misfit dislocations, hot rolling, cold drawing

Abstract

A series of samples of the C45 (0.45 wt.% C) steel was prepared by hot rolling with different thermomechanical history in an industrial-type rolling stage (e.g. rolling temperature and speed, cooling rate). The microstructure of resulting material was ferritic-pearlitic with a pearlite volume fraction ranging from 57 to 90%; the mean interlamellar spacing in the pearlite varied between 180 and 270 nm. An equally-spaced arrangement of misfit dislocations was found at the ferrite/cementite interfaces. The microstrain they generate was observed in the X-ray diffraction by means of anisotropic line broadening; the density of the dislocations was proved to be proportional to the density of the lamellas. The dislocation density was found to correlate with the ultimate tensile strength (UTS) of the steel in the tensile test as well as the density of the lamellas. Upon gradual cold drawing through conical dies, the dislocation density observed in X-ray increased up to about 120 % of elongation, the UTS was still well-following its dependence on the dislocation density, while the density of pearlitic lamellas remained intact. The X-ray diffraction can thus be utilised for an instant and non-destructive estimation of UTS of hot-rolled ferritic-pearlitic steels and cold-drawn steels with moderate grade of cold deformation.

Properties of ferritic-pearlitic steels

Ferritic-pealitic (F-P) steels have a variety of application in construction and reinforcement. Their microstructure consist of proeutectiod primarily crystallised ferritic grains with eutectoid lamellar structure of ferrite and cementite – pearlite. The primary ferrite crystallises predominantly on the grain boundaries of the parent austenite (fcc) grains, the eutectoid is formed at the temperature below 727 °C from the rest austenite. If the cooling regime above this temperature is slow, the carbon concentration in the transforming austenite would reach the maximum value of 0.76 wt.% C, and the amount of primary ferrite would be at maximum. Faster cooling reduces the amount of primary ferrite and raises the resulting *pearlite volume fraction*.

Thus, the mean interlamellar spacing (ILS) in pearlite depends on its formation temperature, the lower below the critical temperature, the smaller the spacing. ILS is proportional either to $(T_C - T)^{-1}$ [1] or to $\exp(T_C - T)$ [2]. A continuous cooling regime will spread the statistical variation of ILS to a wider extent in different *pearlite colonies* (areas with similar orientation of ferrite/cementite and the direction of lamellas), the mean ILS still remains a relevant statistical parameter.

Numerous mechanical studies of fully pearlitic steels revealed that the yield strength (YS,) is inversely proportional to the ILS (S), the so-called Hall-Petch relationship:

$$_0 \quad K \quad S^{\,m_h} \qquad (1)$$

with K dependent on the particular steel composition. The exponent m_h was originally 1/2; this was widely accepted [3, 4], but the extrapolated values of $_0$ often yielded too low or even a negative value, especially for smaller values of S, while taking $m_h = 1$, $_0$ yields reasonable positive values approaching the YS of ferritic steels [5]. The experimental studies on the hypoeutectoid (ferritic-pearlitic) steels however, did not show similar simple relationship between YS and ILS; an ambivalent tendency was found in the dependence on pearlite volume fraction [5].

Recently, self-consistent procedures of stress/strain redistribution between both microstructure constituents were applied [6]. Their applicability, however, is limited to pure ferritic or fully pearlitic steels, or to higher stages of deformation in F-P steels, when they can well reproduce the tensile curves, but at the outset of plastic deformation in F-P steels, the correspondence with the experimental deformation curves is poor.

Motivation

The optimisation of the rolling and drawing process in F-P steel production consists from the ingenious variation of the process parameters (rolling temperature, cooling rate, drawing die shape) to change the microstructure in a desired way. However the microstructure analysis demands metallographical preparation of the specimens, as well as a time demanding analysis of the optical microscopy (OM) images or the scanning electron microscopy (SEM) micrographs to achieve any quantification (pearlite volume fraction, mean ILS). For a certain statistical relevance, large areas must be sampled, i.e. numerous images must be taken and analysed.

The X-ray diffraction (XRD) is, due to its nature, a statistical method over a macroscopically large surface area. The specimen preparation consists from the removal of the surface layer affected by an oxidation or by a cutting procedure. The data analysis methods can be easily automated. The difference from the metallography is that XRD does not detect the microstructure on its typical scale, but it re-

flects its exposure in the variation of the lattice periodicity on the atomic scale. The possibility to employ XRD for the fast analysis and estimation of ultimate tensile strength (UTS) of ferritic pearlitic steels was studied and the results appear to be promising.

Experimental

A set of the C45 (0.45 wt.% of carbon) F-P steel samples was prepared by austenitising at 1200 °C in a furnace in air, hot rolling and cooling. Different input rolling temperatures were achieved by holding the sample at the ambient atmosphere. The samples were rolled up to ten passes in the bi-directional rolling stage (with rolling speed 2 $m.s^{-1}$); some were then introduced into a 4-pass continuous rolling stage (output rolling speed 6 or 30 $m.s^{-1}$) with or without intermediate cooling (air, water). The final cooling procedure was performed either in the air of room temperature or in a molten lead bath of 550 °C. This produces a series of samples with different degree of deformation, different rolling temperature in the first and last passes and with different cooling rate, which affected the pearlite formation. Some samples proceeded post-annealing at 600 °C for 2 hours. A representative set of three samples with different pearlite volume fraction and mean ILS was subjected to a cold drawing procedure through subsequently smaller conical dies.

Afterwards, the samples were cut in mutually perpendicular directions, grinded, polished and metallographically etched. The scanning electron microscopy (SEM) was utilised for evaluation of pearlite volume fraction and mean ILS. For selected specimens, tensile test was performed and its parameters (YS, UTS, ultimate elongation) were evaluated. Few samples were also investigated in transmission electron microscope (TEM) to study the local dislocation arrangement.

The complete sample set was investigated by means of XRD on a URD-6 Bragg-Brentano goniometer equipped with copper anode X-ray tube operated at 40 kV and 30 mA and with a graphite monochromator in the diffracted beam to suppress the effect of iron fluorescence. The divergence slit was 0.8 degrees, the step size 0.02 degrees. The acquisition time was in the range of 10 to 40 seconds per step. The instrumental broadening was determined experimentally using an LaB_6 NIST powder standard.

Data analysis

In the XRD patterns, the ferrite reflections 110, 200, 211, 220, 310 and 222 were fitted by Pearson VII functions. Two mutually shifted Pearson VII functions of the same shape parameters having the intensity ratio 2:1 were used for each reflection to account for the CuK radiation doublet. From their parameters, the interplanar spacings d_{hkl} and integral breadths $_{hkl}$ were calculated. The peaks corresponding to cementite were too weak to give reliable data. The line positions show shifts characteristic for ferrite embedded in pearlite [7] and the integral breadths show an anisotropy which is typical for a dislocation originated broadening [8] (Figure 1).

The squared integral breadths $^2_{hkl}$ were thus fitted using the dependence after [8]:

$$^2_{hkl} \quad ^2_{inst}(\ _{hkl}) \quad ^2_{size} \quad ^2_{disl}(1 \quad qH^2_{hkl})\frac{4}{d_{hkl}} \qquad (2)$$

where $_{inst}$ represents the measured instrumental broadening, $_{size}$ broadening due to finite size of diffracting domains (as a fit parameter, which appears to be negligible) and $_{disl}$ is a root-mean-squared microstrain observed in the crystallographic direction 100 . The parameter q represents anisotropy of the microstrain according to the cubic invariant H_{hkl}:

$$H^2_{hkl} \quad \frac{h^2k^2 \quad h^2l^2 \quad l^2k^2}{(h^2 \quad k^2 \quad l^2)} \qquad (3)$$

Results – hot rolled samples

The anisotropy of the line broadening, q. $^2_{disl}$ from Eq. (2), plotted against the mean squared microstrain $^2_{disl}$ shows various values among the sample series, but the individual values are well correlated (Figure 2). The anisotropy parameter q can thus be considered as practically constant for all of the samples. According to [8], the value of q depends

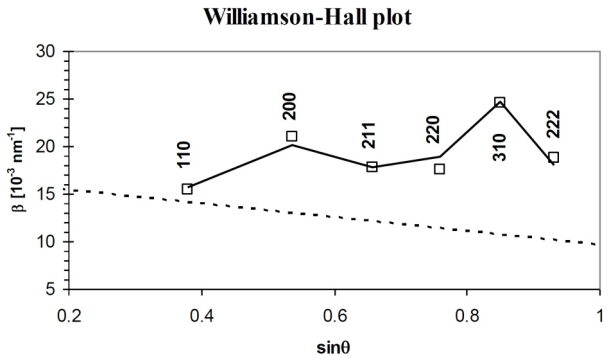

Figure 1. An example of the Williamson-Hall plot showing the effect of dislocation-originated anisotropic broadening. The dashed line represents the instrumental line broadening.

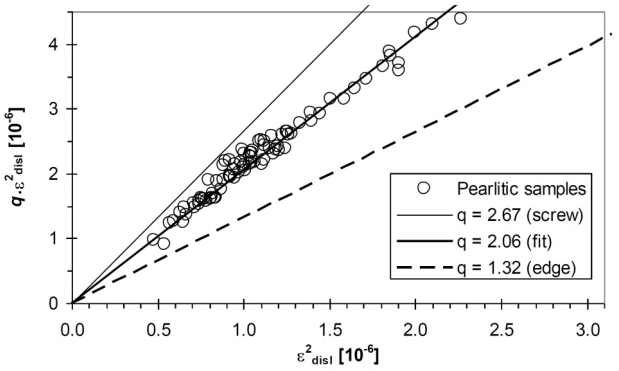

Figure 2. The magnitude of dislocation originated mean squared microstrain anisotropy vs. mean squared microstrain in 100 direction for hot-rolled samples.

on the kind of dislocations. The values of q corresponding to pure edge and pure screw dislocations in bcc iron were indicated in Fig. 2 by the dashed and thin lines, respectively. The thick line uses $q = 2.06$ and represents a best-fit to all of the hot-rolled samples.

The diagram in Figure 2 (and $q = 2.06$) can be interpreted as there are either both types of dislocations in constant statistical occurrence ratio or the character of the dislocations is mixed. According to [8], the mean squared dislocation-originated microstrain corresponds with their density as follows:

$$\varepsilon^2_{disl} \quad \frac{}{8} M^2 b^2 C_{h00} \ , \tag{4}$$

here b represents their Burgers vector magnitude ($\boldsymbol{b} = a_0$ 111 , $a_0 = 2.876$ Å), M is a constant accounting for a dislocation correlation and C_{h00} is a mean dislocation *contrast factor* in 100 crystallographical direction, i.e. the average projection of the dislocation deformation field along the crystallographic basis vector [9]. The exact value of M can hardly be estimated in case of polycrystalline samples, thus an evaluation of the true dislocation density would be questionable; the product of all these constants [(/8)×$M^2b^2C_{h00}$] is in the order of 10^{-22} m^2.

An insight into the dislocation arrangement was mediated by transmission electron microscope. TEM showed quite low dislocation density in the primary ferrite grains, while in the ferritic lamellas of pearlite, a large dislocation density was found on the ferrite/cementite interfaces. They are almost equally spaced within a certain pearlite colony. For sure, these are the misfit dislocations, which help to adopt the lattice incompatibility of both phases having a different structure and certain orientation relationship.

The density of the dislocations in such a colony will be inversely proportional to their mutual distance d_d and to the ILS of the colony. Consequently, the over-all dislocation density will be proportional to the volume fraction of pearlite p and inversely proportional to the mean ILS S and mean distance of misfit dislocations d_d :

$$\frac{2p}{\langle d_d \rangle S}.$$

The distances of the dislocations on the interfaces are in the order of 10 nm, the ILS is about 200 nm, which supposes a dislocation density in the order of 10^{15} m^{-2}, a number well suitable for XRD detection. Following the discussion of Equation (4), the mean squared microstrain produced by such dislocations would be of the order of 10^{-7}, which is in a good agreement with results from XRD (cf. horizontal scale of the diagram in Figure 2).

Correlation may be expected also with the density of the lamellas, which can be evaluated independently from the metallography as = p/S, the proportionality constant being 2/ d_d :

$$\frac{2}{\langle d_d \rangle} \tag{5}$$

The correspondence is illustrated in Figure 4, though it is not perfect.

According to Equation (1), the strength of the pearlite is inversely proportional to its mean ILS. A simplification can be made that in the F-P steel under higher deformation, the UTS is proportional to a weighted average of UTS of both constituents, i.e. to a ferrite strength ($_f$ – including deformation hardening) and pearlite strength (1). The weight coefficients are $(1 - p)$ and p respectively. Then, it can be anticipated that:

$$_f \quad p.K \quad S^{-1} \quad _f \quad K \tag{7}$$

The validity/applicability of Eq. (7) is illustrated in Fig. 5.

Unlike the YS, the simplification is well-fulfilled for UTS, following a tendency described by an equation UTS = (620 + 40×10^6×) MPa also shown in Fig. 5. As-

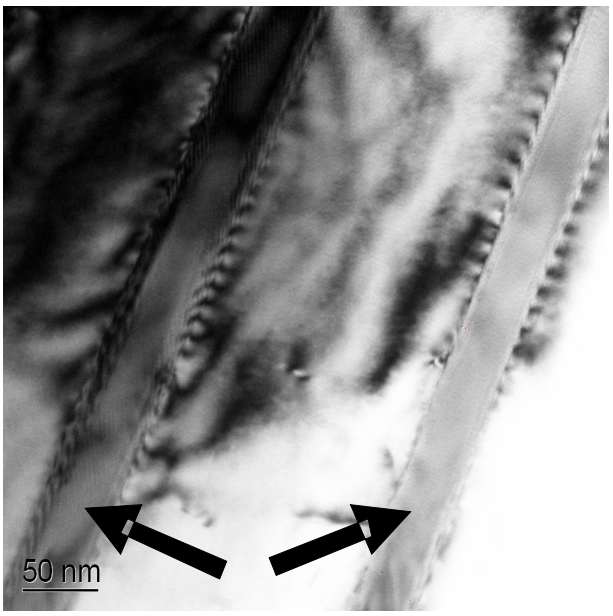

Figure 3. TEM image of cementite lamellas (labelled by arrows) in the pearlite taken in the diffraction contrast. The diffraction contrast of ferrite reveals the deformation fields from misfit dislocations on the interfaces.

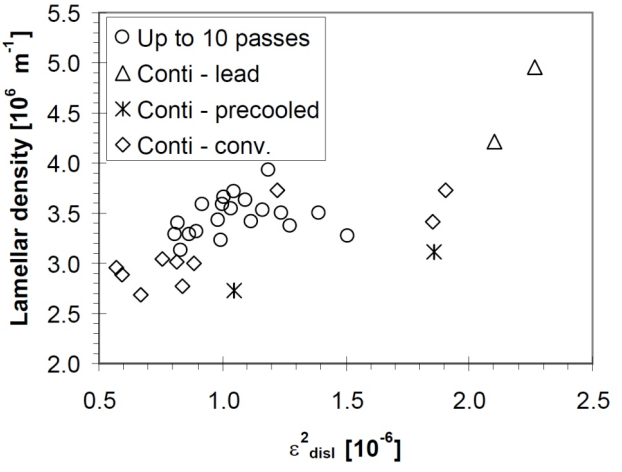

Figure 4. Correlation of lamellar density and dislocation-originated squared microstrain.

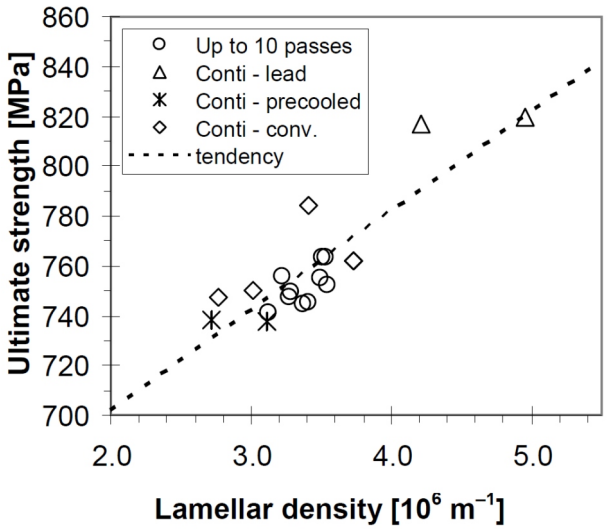

Figure 5. The correlation of ultimate strength with lamellar density determined from metallography.

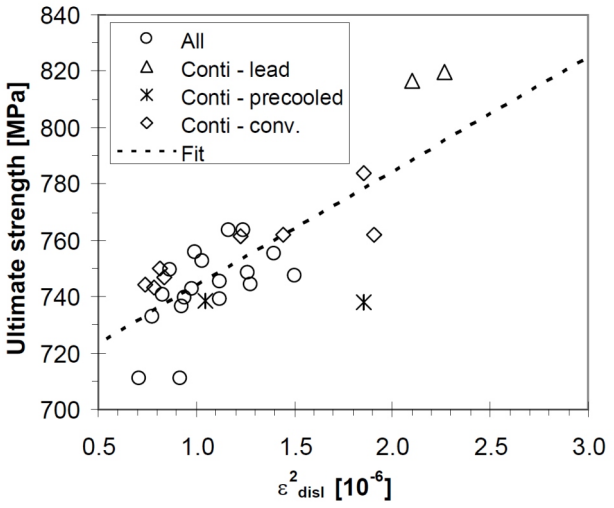

Figure 6. The correlation of ultimate strength with dislocation-originated squared microstrain.

suming the above correlations have been proved, we can look for the correlation of UTS with the dislocation-originated mean squared microstrain $^{2}_{disl}$. The diagram in Figure 6 shows this correlation together with a tendency according to UTS = (700 + 41×10^{6}× $^{2}_{disl}$) MPa.

Results – cold drawn samples

Three samples of the groups depicted by special symbols in Figures 4 to 6 we subjected to a cold drawing procedure. After the first passes of the cold drawing, the pearlite nodules and primary ferrite grains elongate in the drawing direction (DD), the pearlitic lamellas start to reorient along the DD. However, no significant change was observed in their mean ILS. Similarly, the pearlite volume fraction remains intact. This can be explained by the following model. If there is any deformation in pearlite, it has only a shear component along the lamellas; the dislocations do not pass the lamellas. The YS does not vary significantly, while the UTS increases in this region. In the diagram shown in Fig. 5, there would be additional points with the same x-value but with increasing y-value, thus they would lie out of the tendency.

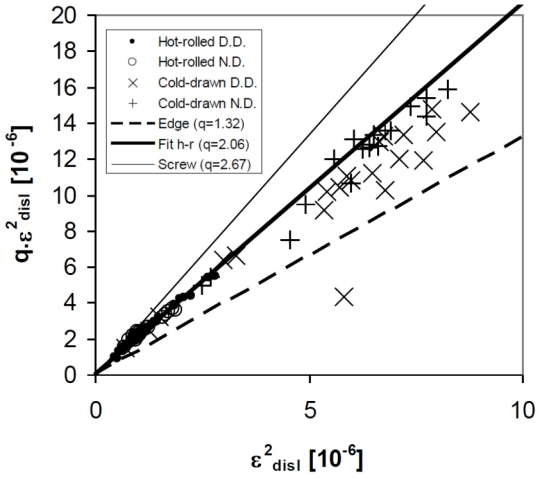

Figure 7. The magnitude of dislocation originated mean squared microstrain anisotropy vs. mean squared microstrain in the 100 direction for hot-rolled and cold drawn samples. The parameter q was determined from measurements in two perpendicular directions along (D.D.) and across (N.D.) rolling/drawing direction.

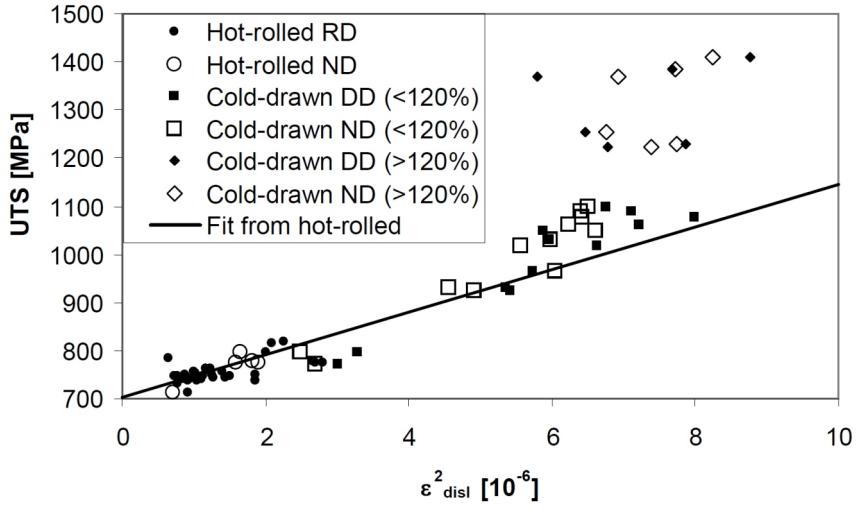

Figure 8. The correlation of ultimate strength with dislocation-originated squared microstrain for cold drawn samples.

However, the mean squared microstrain increases, maintaining practically the same anisotropy as for the hot-rolled samples (Figure 7). The tendency established its correlation with UTS for hot rolled samples (Figure 6) is still well maintained (Figure 8) until about 100% of cold elongation. For larger deformations, a saturation of mean squared microstrain occurs, while the UTS continues rising.

The processes taking place in the deformed steel at the beginning of the cold drawing procedure can be un-

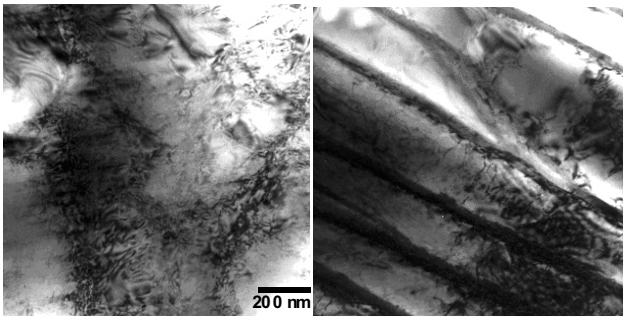

Figure 9. Primary ferrite grain (left) and a pearlitic colony (right) after 10 % of cold elongation.

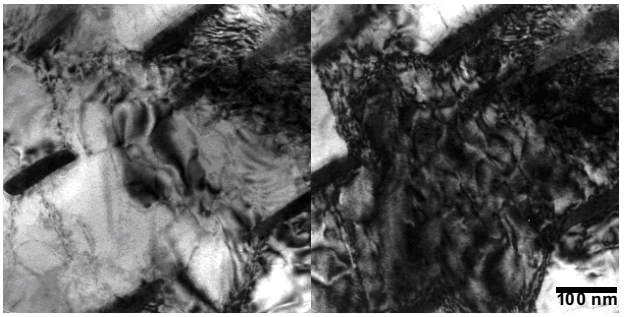

Figure 10. Pearlitic colony after 117 % of cold elongation. This TEM micrograph was taken at two different inclinations of the sample

derstood with the help of TEM. In primary ferrite, apart from still almost dislocation free grains, grains with a large dislocation density start to appear (Figure 9). Even in pearlite, the dislocation density increases inside the lamellas. The occurrence of dislocations is now not limited to the cementite/ferrite interfaces only. The cementite lamellas are still continuous.

This process continues till about 100% of cold elongation, when the dislocation density is already high in all the primary ferrite grains. A new process is introduced – the cementite lamellas start to rupture at the dislocation pile-ups, as illustrated in Figure 10 after 117 % of cold elongation.

This process is accompanied by changes in the shape of tensile curves. The originally different tensile curves for samples with different pearlite volume fraction and mean ILS (Figure 11a) start to change. After a single pass through a die (Figure 11b), the UTS increases, but still the curves show differences in UTS according to their original state. After four drawing steps (Figure 11c), the shape of the curves (and the UTS) coincide into a very similar shape. This is the moment of the mean squared microstrain value saturation.

Subsequent drawing (beyond 100 % elongation) hardens further the samples, the UTS as well as YS then increases. At the same time, the mean ILS starts to drop, but this parameter is already extremely difficult to determine, for that the lamellas are being ruptured gradually.

Discussion

The misfit dislocations, which were observed in the pearlite, and the dislocations introduced by the cold deformation are apparently of a similar type, as can be anticipated from their same/similar microstrain anisotropy (Figure 7). The slightly lower q value observed in the drawing direction can be a consequence of the texture developing during cold deformation, which suppresses the 222 diffraction line along DD. The error of these experimental points is thus higher than for observation in the normal direction.

Although the correlation of lamellar density with the mean squared microstrain is not well pronounced, the correlation of UTS with mean squared microstrain shows a better accordance, even for the cold drawn samples. This can bring us to a conclusion that the hardening effect in

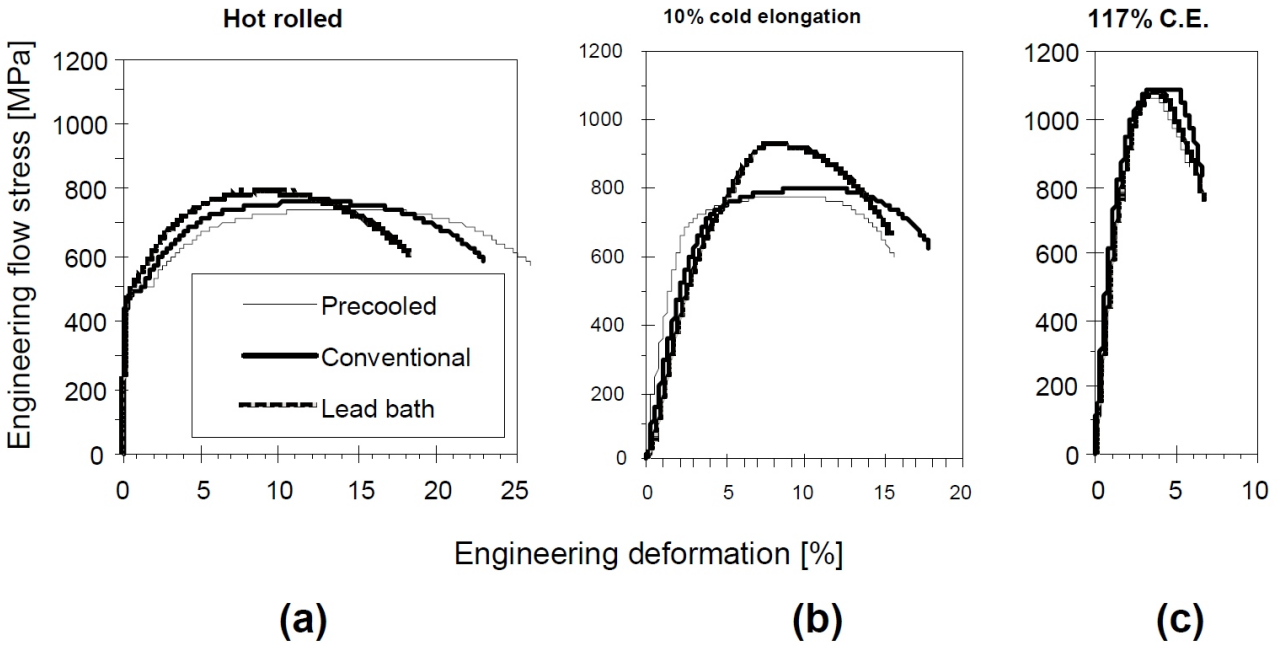

Figure 11. Tensile curves of samples after hot rolling (a), after 10 % of cold elongation (b) and after 117 % of elongation (c) by drawing through conical dies.

pearlite, which is described empirically by Equation (1), is not only caused by the presence of the cementite lamellas, but also by the presence of the misfit dislocations forming at the interfaces. At higher grades of cold deformation, when the dislocation density saturates and the lamellas start to break, this mechanism of hardening becomes subsidiary and the correlation between the UTS and the mean squared microstrain is lost.

However, the extrapolated value of UTS for low microstrains (as well as for the low lamellar densities) is far too high in comparison with pure ferrite (700 MPa versus about 400 MPa). It can be expected that the established linear dependence is not kept for very low dislocation/lamellar densities. A similar effect was already noticed in the literature, as the m_h exponent in (1) was reported to be 1/2 for ILS $S > 540$ nm by Modi et al. [10], while Ray and Mondal [5] found $m_h = 1$ more suitable for $S < 400$ nm, the latter case covers the range of ILS observed in our case.

A shielding effect of the dislocation fields can be expected, as the misfit dislocations have the same Burgers vector and their dislocation lines are parallel. The deformation field will thus not reach much farther then their mutual distances at the interface are. This will lower the effect of the dislocation mobility impedance and thus the YS/UTS values for larger ILS (i.e. for lower lamellar densities).

Conclusions

An arrangement of misfit dislocations on the ferrite/cementite interfaces in pearlite was identified to be a dominant source of microstrain in the hot rolled ferritic-pearlitic steels. The microstrain can be measured by means of X-ray diffraction line broadening and utilised for estimation of ultimate tensile strength of the material for hot-rolled and also for cold-drawn steel below ~ 120 % of cold elongation. The limiting mean squared microstrain, below which the UTS can be determined solely from the XRD is 6×10^{-6}. The key role of dislocation in the pearlite strength was discussed.

References

1. C. Zener, *Trans. AIME*, **167** (1946), 550.
2. R. F. Mehl & W. C. Hagel, *Progr. Met. Phys.*, **6** (1956) 74-134.
3. A. M. Elwazri, P. Wanjara & S. Yue, *Mat. Sci. Eng. A*, **404** (2005) 91-98.
4. J. M. Hyzak & I. M. Bernstein, *Met. Trans. A*, **7** (1976) 1217-1224.
5. K. K. Ray & D. Mondal, *Acta Metall. Mater.*, **39** (1991) 2201-2208.
6. S. Allain & O. Bouaziz, *Mat. Sci. Eng. A*, **496** (2008) 329-336.
7. D. Šimek, D. Rafaja, M. Motylenko, V. Klemm, G. Schreiber, A. Brethfeld & G. Lehmann, *Steel Res. Int.*, **79** (2008) 800-806.
8. T. Ungár, I. Dragomir, Á. Révész & A. Borbély, *J. Appl. Cryst.*, **32** (1999) 992-1002.
9. R. Kužel, *Z. Kristallogr. Suppl.*, **23** (2006) 75-80.
10. O. P. Modi, N. Deshmukh, D. P. Mondal, A. K. Jha, A. H. Yegneswaran & H. K. Khaira, *Mater. Char.*, **46** (2001) 347-352